Chemical Principles of the Sulfidation of Tungsten Oxides

A. J. van der Vlies, R. Prins, and Th. Weber*

Laboratory for Technical Chemistry, Swiss Federal Institute of Technology (ETH), 8093 Zurich, Switzerland

Received: April 11, 2002; In Final Form: June 22, 2002

The sulfidation of crystalline *m*-WO_3 and WO_3•H_2O and the thermal decomposition of $(NH_4)_2WO_2S_2$ to an $\{WOS_2\}$ oxysulfide were studied by means of X-ray powder diffraction, quick extended X-ray absorption fine structure, and infrared emission spectroscopy. Several of the basic steps in the sulfidation reactions of *m*-WO_3 and WO_3•H_2O were resolved and explained in terms of the structures of the oxides. In both cases, the sulfidation reaction follows the same general route, starting at low temperatures with the reduction of the crystalline oxides by H_2S to give hydrogen tungsten bronzes. Only after this reduction can sulfur be incorporated into the oxide structure. At higher temperatures the hydrogen tungsten bronzes transform into shear oxides. Oxygen−sulfur exchange processes on the surface proceed at a higher rate, and *shear oxysulfide* phases form. Further incorporation of sulfur leads to oxysulfide intermediates with higher S:W ratios. W−S redox reactions eventually transform the oxysulfidic phase into WS_2.

Introduction

Catalytic hydrotreating of oil feedstocks for the removal of sulfur, nitrogen, and heavy metals are very important refinery processes that protect noble metal catalysts in downstream processes, and are increasingly important with respect to the environment. Compounds containing sulfur and nitrogen in crude oil contribute to the formation of acid rain and photosmog in the form of SO_2 and NO_x. Therefore, lowering the sulfur and nitrogen contents in fuels has become increasingly important. By the year 2005 the level of sulfur in diesel oil must be reduced to less than 50 ppm.[1] To meet these requirements, the performance of the catalysts used in these processes must be improved.

The catalysts used in hydrotreating processes are MoS_2 and WS_2 phases supported on Al_2O_3 to which nickel or cobalt are added as promoters.[2,3] Molybdenum-based catalysts are normally used because they are cheaper than their tungsten-based counterparts. Furthermore, molybdenum-based catalysts are more active in the traditional hydrotreating process. On the other hand, tungsten-based catalysts have excellent hydrogenation properties. This makes them particularly interesting for deep hydrodesulfurization (e.g., removal of sulfur from alkyl substituted dibenzothiophenes) and hydrodenitrogenation where hydrogenation of the aromatic rings is the critical step.

Tungsten-based catalysts are prepared by impregnating Al_2O_3 with ammonium *meta*- or *para*-tungstate, followed by drying and calcination. During the calcination step an amorphous WO_3-phase forms. The active sulfide catalyst is obtained by sulfidation of this oxidic precursor in H_2S/H_2.

The sulfidation reaction is a crucial step in the preparation of tungsten sulfide catalysts, because it has a profound influence on the (surface) structure and on the dispersion of the catalytically active particles. The major difficulty in understanding the mechanism of this reaction is the amorphous nature of the WO_3-type phases in the catalyst precursor. The variety of local W−O coordination environments, which form randomly during the preparation of the catalyst precursor, is a major obstacle to understanding the sulfidation reaction.

This contribution describes the chemistry and structures of intermediate phases of the sulfidation of crystalline *m*-WO_3 and WO_3•H_2O and provides a basis for understanding the sulfidation reaction of WO_3/Al_2O_3 catalyst precursors. The exchange of oxygen from the oxides for sulfur leads to the formation of oxysulfide phases. Thus, the complex $(NH_4)_2WO_2S_2$, which can be decomposed to an oxysulfide phase of the composition $\{WOS_2\}$, was studied as well.

Experimental Section

Synthesis of Compounds. *m*-WO_3 was used as supplied (Fluka, 99.99%). $(NH_4)_2WO_2S_2$[4] and WO_3•H_2O[5] were prepared according to published procedures.

XRD Measurements. XRD powder diffraction patterns from $2\theta = 5$ to 60° were measured with a Siemens D5000 diffractometer using Cu Kα radiation ($\lambda = 1.5406$ Å). Sulfidation of the crystalline solids, i.e., *m*-WO_3 and WO_3•H_2O, was done in a flow of 10% H_2S in H_2 (60 mL/min) in a quartz reactor. The samples were heated to the desired temperatures at a rate of 2 °C/min and kept at this temperature for 2 h, cooled in the H_2S/H_2 gas mixture, and then flushed with Ar for 15 min. The powder patterns were recorded immediately afterward under ambient conditions.

Quick EXAFS Measurements. The quick EXAFS measurements were carried out at the X1 (ROMO II) beamline of HASYLAB (Hamburg, Germany), which is equipped with a monochromator consisting of a pair of Si(111) crystals to measure the W L_{III} edge. The *k* range used for the analysis of the data was 3 to 14 $Å^{-1}$. *m*-WO_3 and WO_3•H_2O were mixed with carbon, pressed into a wafer, and placed in an *in situ* EXAFS cell. After collecting three spectra of the samples in He atmosphere at room temperature, sulfidation was started. The sample was heated in a stream of H_2S/H_2 to 400 °C (3 °C/min) and kept at this temperature for 30 min. Each EXAFS scan took 6 min, which corresponds to a temperature interval

* Author to whom correspondence should be addressed at Laboratory for Technical Chemistry, Swiss Federal Institute of Technology, ETH-Hönggerberg, HC1, D131, CH-8093 Zurich, Switzerland. Tel.: + 41 1 632 30 43. Fax: + 41 1 632 11 62. E-mail: thomas.weber@tech.chem.ethz.ch.

10.1021/jp020961v CCC: $22.00
Published on Web 08/20/2002

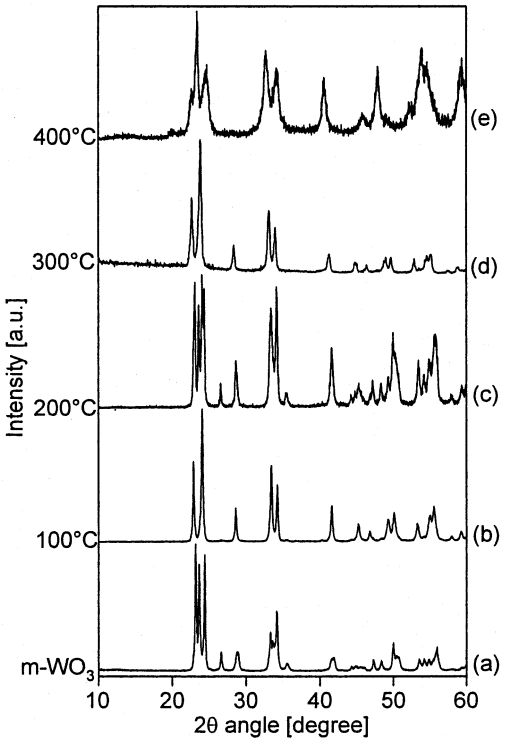

Figure 1. XRD patterns of crystalline *m*-WO_3 (a) and its products after sulfidation (10% H_2S/H_2, 2 h) at the indicated temperatures (b−e).

of 18 °C during the temperature ramp. The XDAP program (version 2.2.2) was used to analyze and process the data.[6,7] The preedge background was approximated by a modified Victoreen function, and the background was subtracted using a cubic spline routine. The spectra were normalized by the edge jump. The k^3-weighted EXAFS functions were Fourier transformed.

IR Spectroscopy. Fourier transform infrared spectra were obtained with a Bruker Equinox 55 spectrometer equipped with a DTGS detector and a KBr beam splitter for the mid-infrared region. Data collection and processing were controlled by the OPUS 2.2 software (Bruker). The transmission infrared spectrum of $(NH_4)_2WO_2S_2$ was measured with a spectral resolution of 4 cm^{-1}. The powdered sample was diluted with CsI and pressed into a self-supporting disk.

Infrared emission studies were conducted in a specially designed IR emission cell similar to those in refs 8 and 9. The samples were applied as thin layers on the surface of the cell. About 2 mg of the sample and 0.7 mL of 2-propanol were shaken in a vibrating mill. The resulting suspension was spread on the surface of the stainless steel sample deposition area, the liquid was slowly evaporated, and the sample holder was mounted in the cell. For the thermal decomposition of $(NH_4)_2WO_2S_2$, the emission cell was purged with Ar and heated (10 °C/min) to the different temperatures. The sample was kept at the respective temperature for 15 min before the spectra were collected. Each spectrum is the sum of 512 scans with a spectral resolution of 8 cm^{-1}. The sample holder (without the sample) at the different temperatures served as the background spectrum.

Results

Sulfidation of *m*-WO_3 and $WO_3 \bullet H_2O$. *XRD.* Figure 1 shows the X-ray powder diffraction patterns of *m*-WO_3 and its sulfidation products at different sulfidation temperatures. The powder patterns obtained after sulfidation at 100, 200, and 300 °C are similar to that of the tetragonal tungsten bronze $H_{0.23}WO_3$. At a sulfidation temperature of 200 °C, reflections due to *m*-WO_3 are also visible. After sulfidation at 400 °C, the powder pattern is very similar to that of the shear oxide $W_{20}O_{58}$.

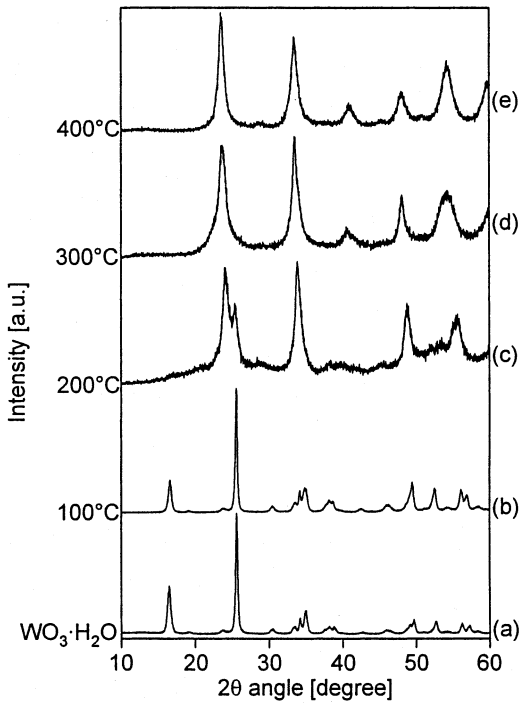

Figure 2. XRD patterns of crystalline $WO_3 \bullet H_2O$ (a) and of its production after sulfidation (10% H_2S/H_2, 2 h) at the indicated temperatures (b−e).

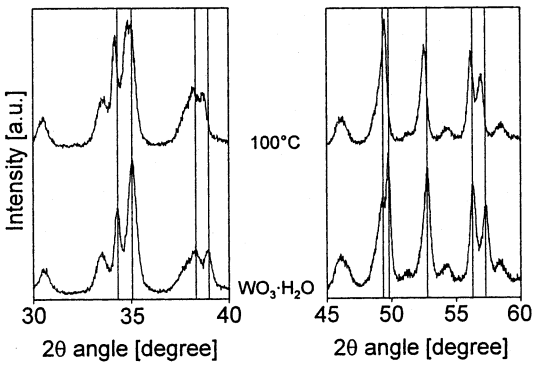

Figure 3. XRD patterns of crystalline $WO_3 \bullet H_2O$ (a) and of the material obtained after sulfidation at 100 °C (b).

Figure 2 shows the powder diffraction data of $WO_3 \bullet H_2O$ and the sulfidation intermediates at different temperatures. After sulfidation at 100 °C the powder pattern is slightly different from that of the starting material, i.e., some reflections have shifted, whereas others remained at their original positions (Figure 3). No matching XRD were found in the JCPDS database. At sulfidation temperatures above 100 °C, the powder patterns show a strong broadening of the reflections, which hinders an unequivocal assignment. The color of both oxides during sulfidation changed from yellow to gray-blue to gray-black.

Quick EXAFS. Figure 4 shows the quick EXAFS data of the sulfidation of *m*-WO_3. The distances are not phase-corrected and thus differ from those determined by crystallographic methods. To discriminate between crystallographic and EXAFS data, the distances obtained by quick EXAFS are in *italics*. The quick EXAFS spectrum of *m*-WO_3 shows a broad signal at *1.2* Å together with two weak signals at *2.8* and *3.5* Å. The structure of *m*-WO_3 is made up of distorted corner-sharing [WO_6]

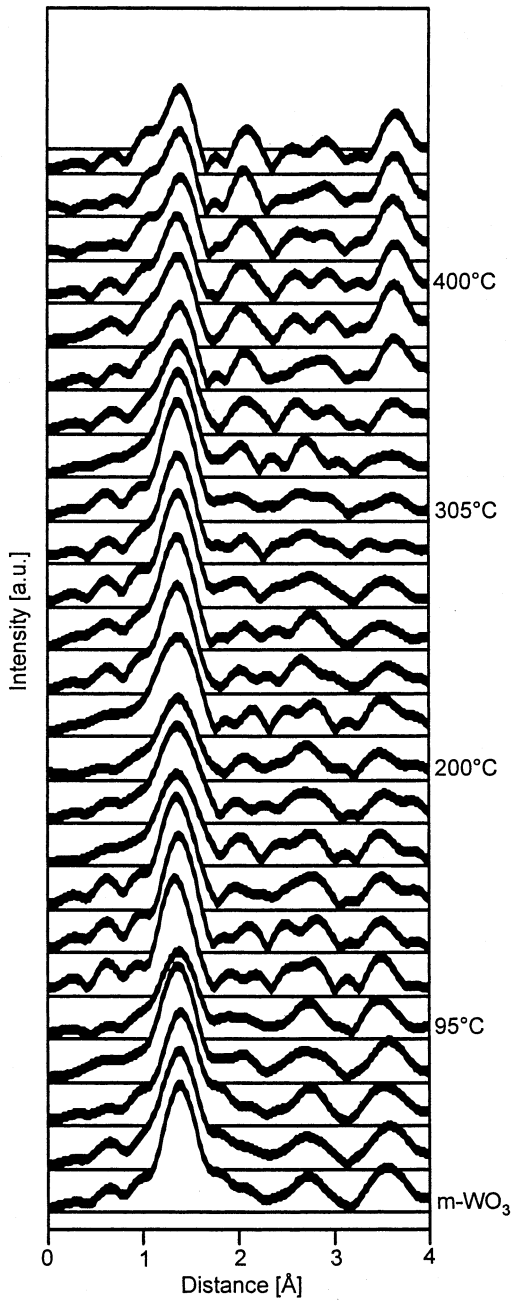

Figure 4. Fourier transform of the W L_{III} edge k^3-weighted quick EXAFS spectrum of *m*-WO_3 and after sulfidation (10% H_2S/H_2) at the indicated temperatures.

octahedra (Figure 5), with W−O distances between 1.72 and 2.16 Å.[10] Taking the broadness of the EXAFS signal and the phase shift into account, the signal at *1.2* Å can be assigned to these W−O distances. Even though *m*-WO_3 has W−O distances between 3.70 and 3.86 Å, the signal at *3.5* Å does not correspond to these W−O distances. Because of its low atomic mass, oxygen does not contribute to the signal at *3.5* Å. It is therefore, due only to W−W distances, which are between 3.69 and 3.86 Å in *m*-WO_3. The origin of the signal at around *2.8* Å is unclear, because there are no such distances in *m*-WO_3.

At sulfidation temperatures below 350 °C the quick EXAFS data do not change significantly, i.e., the signals at *1.2* and *3.5* *Å* remain at the same position. The XRD data show the presence of the tungsten bronze $H_{0.23}WO_3$ in this temperature region. In $H_{0.23}WO_3$, the W−O distances (1.86−1.94 Å) and the W−W distances (3.73−3.88 Å)[17] do not differ significantly from those

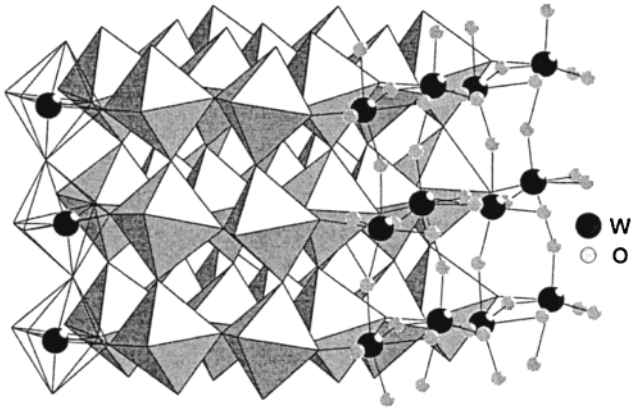

Figure 5. Structure of crystalline *m*-WO_3.

of *m*-WO_3, which explains why the signals at *1.2* and *3.5* Å remain at the same positions.

At sulfidation temperatures above 350 °C two new signals appear at *2.0* and *3.6* Å; their intensities increase with increasing sulfidation temperature. The signal at *2.0* Å is due to the incorporation of sulfur into the oxide lattice and is thus assigned to a W−S contribution. At this temperature, XRD shows the presence of the shear oxide $W_{20}O_{58}$. $W_{20}O_{58}$ contains shorter (3.28−3.33 Å) and longer (3.75−3.80 Å) W−W distances,[11] whereas most of the W−W distances are in the range of 3.75 to 3.80 Å. We therefore consider the signal at *3.6 Å* to be due to W−W distances of the $W_{20}O_{58}$ shear oxide. This means that the structure of the sulfidation intermediate at 350 °C is the same as that of the $W_{20}O_{58}$ shear oxide, with some of the oxygen atoms being replaced by sulfur. Because of this particular structural property we refer to this phase as a *shear oxysulfide*.

The quick EXAFS data of $WO_3 \bullet H_2O$ (Figure 6) show three distances at *1.2*, *1.8*, and *3.5* Å. $WO_3 \bullet H_2O$ consists of layers of [WO_6] octahedra, sharing the same equatorial oxygen[12] (Figure 7). One of the axial positions is occupied by a water ligand, which forms a hydrogen bond with an oxygen atom in the next layer. The W−O distances are between 1.69 and 2.34 Å. In the axial positions, the W−O bond length of W═O is 1.9 Å and that of W−OH_2 is 2.3 Å. We assign the signal at *1.2* Å to the four equatorial and the axial tungsten−oxygen distances, whereas the signal at *1.8* Å is due to the W−OH_2 distance. The signal at *3.5* Å is due to W−W distances at 3.72 Å.

Upon sulfidation, the signals at *1.2* and *1.8* Å broaden and merge, whereas the contribution at *3.5* Å disappears at sulfidation temperatures above 200 °C. A signal at *2.0* Å occurs at sulfidation temperatures of 350 °C and higher. While the intensity of this signal increases rapidly, the contribution at *1.6* Å slowly disappears. The signal at *2.0* Å is due to the incorporation of sulfur and is assigned to a W−S distance. The incorporation of sulfur proceeds at the expense of oxygen. For this reason the W−O contribution at *1.6* Å decreases with increasing amounts of incorporated sulfur.

Thermal Decomposition of $(NH_4)_2WO_2S_2$. The complex $(NH_4)_2WO_2S_2$ decomposes thermally to an oxysulfide phase of the stoichiometry {WOS_2} according to[13]

$$(NH_4)_2WO_2S_2 \rightarrow \{WOS_2\} + H_2O + 2NH_3 \qquad (1)$$

Figure 8 shows infrared spectra of $(NH_4)_2WO_2S_2$ and its decomposition products at the indicated temperatures. The absorption IR spectrum of $(NH_4)_2WO_2S_2$ (Figure 8a) shows the characteristic bands of the $WO_2S_2^{2-}$ complex anion[14] (see Table 1) together with the δ(H−N−H) bending vibration of the NH_4^+ cation.[15] Upon decomposition, the well-defined W═O_t and W═

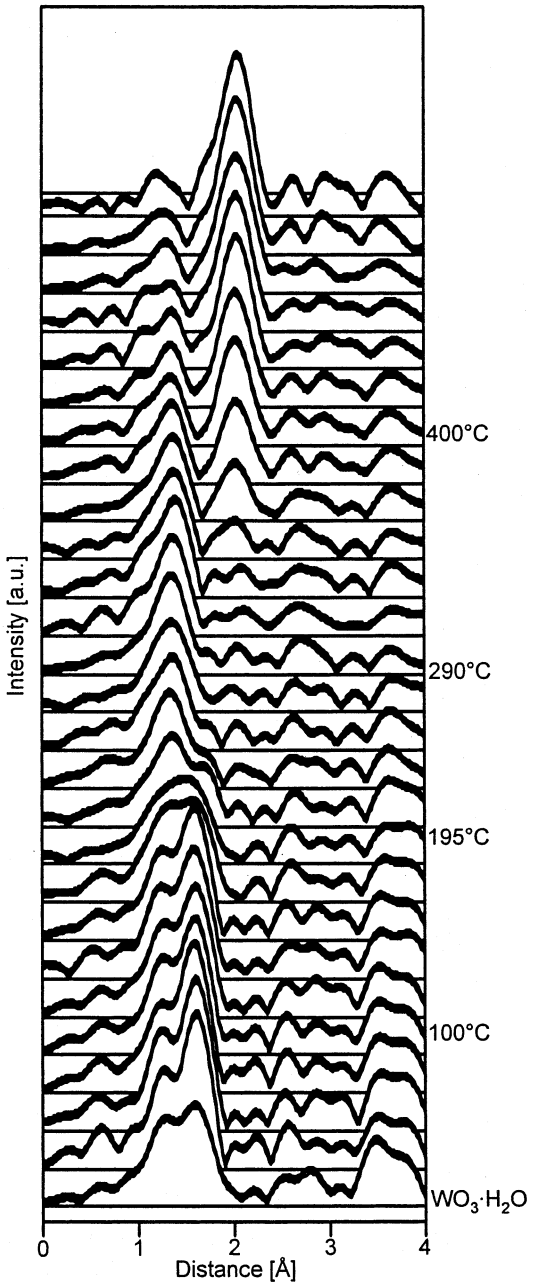

Figure 6. Fourier transform of the W L_{III} edge k^3-weighted quick EXAFS spectrum of $WO_3 \bullet H_2O$ and after sulfidation (10% H_2S/H_2) at the indicated temperatures.

S_t bonds of the complex are replaced by less well-defined W−O and W−S bonds with different bond orders. The decomposition of the complex is complete above 200 °C, as can be seen from the absence of the band due to the δ(H−N−H) bending vibration of the NH_4^+ cation around 1400 cm^{-1}. As temperature increases, the bands due to W−O stretching vibrations (1000 to 600 cm^{-1}) broaden. The band at 980 cm^{-1} in the spectrum at 250 °C is of particular interest, and is typically due to the ν(W═O_t) stretching vibration. We assign the broad band to the ν(W−O) stretching vibrations of W−O−W structures, i.e., of oxygen in bridging coordination types. Upon decomposition, changes also take place in the region of the W−S vibrations between 600 and 400 cm^{-1}. At 250 °C a band at 521 cm^{-1} is visible, which is typical of the ν(S−S) stretching vibration of S_2^{2-} ligands in the terminal coordination mode. A weak shoulder is visible at 559 cm^{-1}, suggesting the presence of S_2^{2-} ligands in bridging coordination types. This would mean that W−S

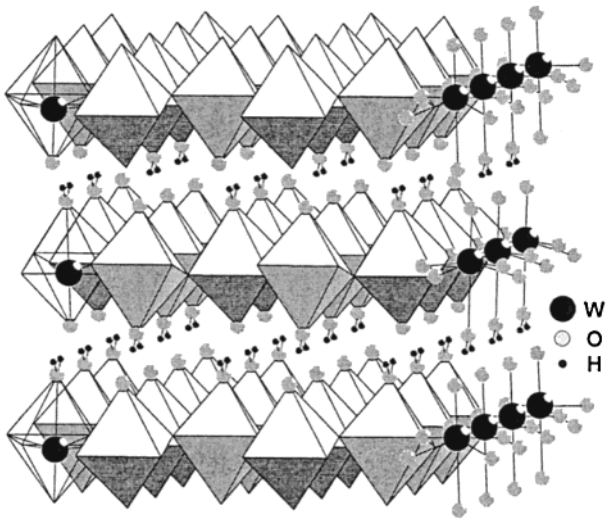

Figure 7. Structure of crystalline $WO_3 \bullet H_2O$.

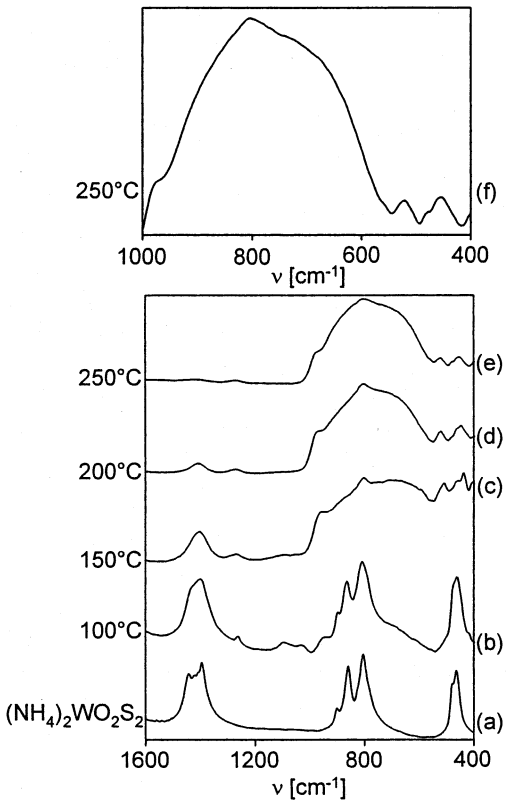

Figure 8. Transmission infrared spectrum of $(NH_4)_2WO_2S_2$ (a) and emission infrared spectra as obtained after thermal decomposition (Ar, 15 min) at the indicated temperatures (b−f).

redox processes took place, during which disulfide species formed by oxidation of the S^{2-} ligands of the starting material according to

$$2S^{2-} \rightarrow S_2^{2-} + 2e^- \qquad (2)$$

The emission infrared spectra clearly show that the majority of the S_2^{2-} ligands of the {WOS_2} phase are present in the terminal coordination mode. The band at 455 cm^{-1} is due to the ν(W−S) stretching vibration of {W−S−W} fragments. We conclude that the {WOS_2} oxysulfide phase contains oxygen in terminal and bridging coordination types and sulfur as S^{2-} and S_2^{2-}.

TABLE 1: Infrared Data of $(NH_4)_2WO_2S_2$ and Its Decomposition Intermediates at the Indicated Temperatures[a]

$(NH_4)_2WO_2S_2$ [cm^{-1}]	assignment	100 °C [cm^{-1}]	150 °C [cm^{-1}]	200 °C [cm^{-1}]	250 °C [cm^{-1}]
		948 (m)	956 (m)	976 (m)	980 (m)
901 (m)		898 (s)			
860 (vs)	$\nu_s(WO) = \nu_1(A_1)$	864 (vs)			
804 (vs)	$\nu_{as}(WO) = \nu_6(B_1)$	806 (vs)	802 (vs)	802 (vs)	802 (vs)
					559 (sh)
			520 (sh)	521 (vs)	521 (s)
			509 (vs)		
478 (vs)	$\nu_s(WS) = \nu_2(A_1)$	474 (sh)	478 (sh)	478 (sh)	478 (sh)
464 (vs)	$\nu_{as}(WS) = \nu_8(B_2)$	462 (vs)	459 (vs)	459 (s)	455 (s)
				447 (s)	
			435 (vs)		436 (sh)
		420 (w)	424 (sh)	424 (sh)	
			405 (s)		

[a] (vs) = very strong, (s) = strong, (m) = medium, (w) = weak, (sh) = shoulder.

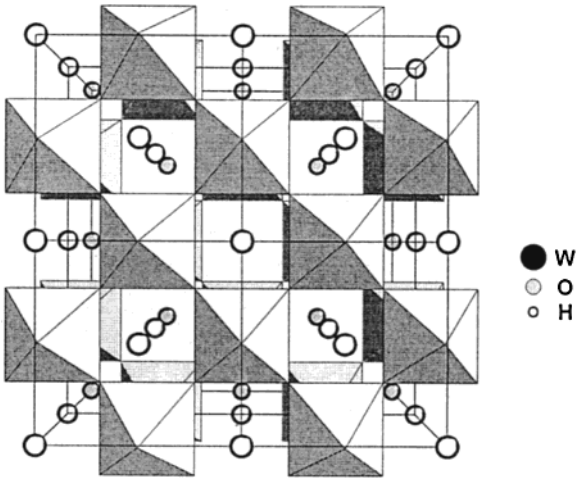

Figure 9. Structure of crystalline $H_{0.23}WO_3$.

Discussion

We will discuss the chemical principles of the sulfidation reactions of the crystalline solids *m*-WO_3 and $WO_3 \bullet H_2O$. Since no literature data is available about the sulfidation of the hydrate phase, the sulfidation reaction of *m*-WO_3 will be described and the results used to describe the sulfidation of $WO_3 \bullet H_2O$.

Sulfidation of *m*-WO_3. The most important results of the sulfidation of *m*-WO_3 can be summarized as follows:

1. The initial reaction of *m*-WO_3 is reduction to the tungsten bronze $H_{0.23}WO_3$.

2. $H_{0.23}WO_3$ subsequently transforms into the shear oxide $W_{20}O_{58}$, and sulfur is incorporated into the shear oxide structure forming a *shear oxysulfide*.

3. Tungsten oxysulfide intermediates contain oxygen in terminal and bridging coordination types and sulfur as S^{2-} and S_2^{2-}. While S^{2-} is mainly present in W−S−W structures, S_2^{2-} ligands predominantly occur in the terminal coordination mode.

At sulfidation temperatures between 100 and 300 °C the powder diffraction data clearly show that *m*-WO_3 is transformed into the tetragonal tungsten bronze $H_{0.23}WO_3$, in which 23% of the tungsten centers are present in the 5+ state. This finding is in line with the results of a previous study,[16] in which we demonstrated with XPS that the first step in the sulfidation of *m*-WO_3 is the reduction of tungsten centers without incorporation of sulfur into the oxide lattice.

Figure 9 shows the structure of $H_{0.23}WO_3$. It consists of corner-sharing [WO_6] octahedra forming a distorted perovskite lattice, in which hydrogen atoms occupy the interstitial positions.[17] As can be seen from comparing the structure of *m*-WO_3 (Figure 5) with that of tetragonal $H_{0.23}WO_3$, the incorporation of protons into the structure reduces the distortion of the [WO_6] octahedra. Tetragonal $H_{0.23}WO_3$ belongs to a class of oxide bronzes (A_xMO_y), in which an electropositive metal A (or hydrogen) is inserted into the oxide lattice of a transition metal M. The oxide lattice is reduced by the valence electrons of the metal or hydrogen. Depending on the stoichiometry, i.e., the value of *x*, these electrons are either localized at the transition metal M or are delocalized in energy bands of the MO_y lattice, leading to semiconducting or conducting bronzes, respectively. In the case of tungsten, hydrogen bronzes are known up to a stoichiometry of $H_{0.60}WO_3$, i.e., $0 < x \leq 0.60$. With increasing *x*, changes in the crystal structures take place from orthorhombic ($x < 0.10$) to tetragonal B ($0.15 < x < 0.23$), tetragonal A ($0.33 < x < 0.50$), and cubic ($x > 0.47$). Depending on the hydrogen stoichiometry, the color of the phases differ, e.g., blue for $x = 0.23$[17] and red for $x = 0.60$.[18] H_xWO_3-type bronzes can be synthesized by reactions of WO_3 with H_2 in the presence of Pt or Pd,[19−21] with atomic[22] or nascent hydrogen[17,18,23−25] as well as by electrochemical means.[26−28] Tungsten bronzes with low hydrogen contents are accessible by controlled oxidation of hydrogen-rich bronzes[18,23,29] and are very sensitive toward further oxidation to WO_3. This might explain why XRD shows reflections due to *m*-WO_3 after sulfidation at 200 °C. Since the XRD patterns were obtained under ambient conditions, surface oxidation of the samples cannot be excluded. To verify this hypothesis, we exposed the sample obtained after sulfidation at 100 °C to air for one week. The resulting XRD pattern is similar to that of *m*-WO_3.

Ampe et al. observed the formation of the tungsten bronze $H_{0.10}WO_3$ by reaction of WO_3 with H_2S between 60 and 240 °C.[30] This shows that the reaction of *m*-WO_3 with H_2S yields a tungsten bronze, regardless of the reaction conditions, i.e., either pure H_2S or H_2/H_2S. We therefore conclude that $H_{0.23}WO_3$ is the first intermediate in the sulfidation of *m*-WO_3.

From XPS we know that sulfur is incorporated into the oxide lattice only if about 20% of the tungsten centers are reduced from $W^{VI} \rightarrow W^{V}$.[16] In contrast to the sulfidation of molybdenum oxides an exchange of oxygen for sulfur according to[9]

$$W^{VI} = O_t + H_2S \rightarrow W^{VI} = S_t + H_2O \qquad (3)$$

cannot occur without a preceding reduction of W^{VI} to W^{V}.[16] This is due to the rather high W−O bond energy, which must be decreased before an exchange of oxygen for sulfur (reaction 3) can take place. It is known from solution chemistry that

protonation weakens the metal−oxygen bonds and has the effect of activating the metal coordination sphere both for substitution and addition.[31]

The positions of the hydrogen atoms in the tungsten bronzes have not been determined unequivocally. In view of the structures of the deuterium-containing derivatives,[32] the hydrogen bronzes can be described as $WO_{3-x}(OH)_x$. This means that W═O fragments are converted into W−OH entities by protonation. The W−OH bonds are sufficiently reactive for exchange reactions of oxygen for sulfur to take place. Analogous to the chemistry in solution we propose an associative substitution mechanism where H_2S is added to the coordination sphere of tungsten under simultaneous release of water according to[31]

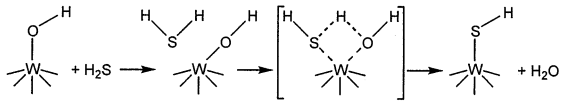

(4)

The formed W−SH fragment is not stable at higher temperatures (a general property of transition-metal complexes with SH^- ligands [33]) and undergoes further reactions during which W═S and W−S−W structures are formed, depending on the coordination environment of the neighboring W centers. W−SH reacts with a W═O fragment to form W═S according to

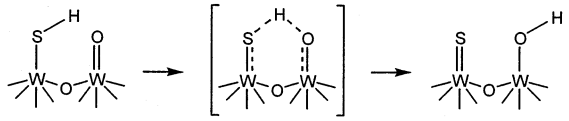
(5)

or with another W−SH group to form W−S−W structures.[31]

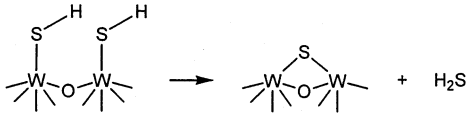

(6)

The mechanism described thus far reflects the situation up to a sulfidation temperature of 300 °C. Once the tungsten bronze has formed, reactions 4 to 6 proceed on the surface of the particles, while, according to XRD (Figure 1), the interior is still that of $H_{0.23}WO_3$. This means that reactions of the oxidic bulk and the oxysulfidic surface still proceed independently of each other. While $H_{0.23}WO_3$ converts into $W_{20}O_{58}$ (vide infra), the tungsten−sulfur surface species undergo redox reactions, as we demonstrated by XPS:[16]

Tungsten centers at edge positions of the particles possess two terminally bonded S^{2-} ligands (after oxygen−sulfur exchange), which undergo a redox process during which terminal disulfide ligands form:

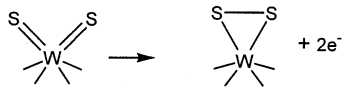

(7)

Two neighboring W═S fragments undergo a metal−ligand redox process, during which a bridging disulfide ligand forms:

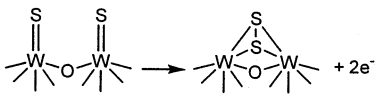

(8)

Both redox reactions provide two electrons, which are used for the reduction of tungsten. Bridging disulfide ligands are known to be unstable in the H_2/H_2S gas mixture at such high temperatures and react with H_2 as follows:[8,9]

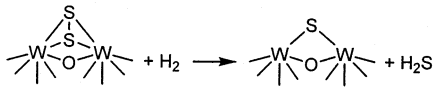

(9)

At sulfidation temperatures above 350 °C the powder diffraction pattern shows that $H_{0.23}WO_3$ has converted into the shear oxide $W_{20}O_{58}$, which is the next bulk intermediate in the sulfidation of *m*-WO_3.

Some of the [WO_6] octahedra of shear oxides share edges instead of only corners.[11,34] In this way, the highly ordered homologous series W_nO_{3n-1} and W_nO_{3n-2} are obtained instead of grossly nonstoichiometric phases. The structure of $W_{20}O_{58}$ is shown in Figure 10a. For the sake of clarity, Figure 10b shows the projection of one layer, demonstrating the edge sharing of some of the [WO_6] octahedra. Edge sharing and corner sharing explain why $W_{20}O_{58}$ has shorter (edge sharing octahedra) and longer W−W distances (corner sharing octahedra), as mentioned above. As a consequence of the oxygen deficiency, some of the tungsten atoms are reduced (20% in $W_{20}O_{58}$) from $W^{VI} \rightarrow W^{V}$. This means that the degree of reduction of tungsten centers in $W_{20}O_{58}$ and $H_{0.23}WO_3$ is similar.

$W_{20}O_{58}$ as an intermediate in the sulfidation of *m*-WO_3 was also observed by Massoth and Bidlack,[35] who studied the sulfidation of *m*-WO_3 in H_2S/H_2 between 260 and 510 °C at different pressures. After sulfidation at 510 °C for 2 h, XRD revealed reflections due to WS_2 and $W_{20}O_{58}$. These authors concluded that *m*-WO_3 reduces quickly to $W_{20}O_{58}$, which then sulfides more slowly to WS_2. The transformation of $H_{0.23}WO_3$ into $W_{20}O_{58}$ at sulfidation temperatures above 350 °C is in line with the well-known instability of hydrogen tungsten bronzes, which decompose at higher temperatures in a vacuum according to[29]

$$H_xWO_3 \rightarrow pH_2 + mH_2O + WO_{3-m} \qquad (10)$$

with *p* determined by measuring the volume of released hydrogen and *m* by measuring the increase in weight after oxidation of WO_{3-m} into WO_3 ($x = (p + m)/2$).

At sulfidation temperatures of 400 °C, the interior of the particles consists mainly of $W_{20}O_{58}$, whereas the surface is enriched with sulfur as a consequence of reactions 4 to 9. The formal composition of this *shear oxysulfide* phase is $\{W_{20}O_{58-x}S_x\}$. This structure may remain intact up to a W:S ratio of 1:1. Further incorporation of sulfur leads to oxysulfide intermediates with higher S:W ratios, which can no longer have a *shear oxysulfide* structure.

To learn more about the properties of oxysulfide phases with a high S:W ratio we investigated the $\{WOS_2\}$ phase, which was prepared by thermal decomposition of the complex $(NH_4)_2WO_2S_2$ (reaction 1). The first reaction step in the formation of this phase is a proton transfer from the two NH_4^+ cations to one of the O^{2-} ligands of the $WO_2S_2^{2-}$ anion, producing NH_3 and a neutral $\{S_2WOH_2O\}$ intermediate. The latter is unstable, releases H_2O, and aggregates. The infrared data presented here are complementary and in agreement with Raman data we reported before.[16] The IR spectrum in Figure 8f reveals that the $\{WOS_2\}$ phase contains W−O−W and W−S−W fragments. The most remarkable and important characteristic of the amorphous $\{WOS_2\}$ phase, however, is that it contains oxygen in terminal positions, W═O_t, as indicated by the band at 980 cm^{-1} in the IR spectrum (Figure 8f). The bands at 455 and 521 cm^{-1} as well as the weak shoulder at 559 cm^{-1} show that sulfur is present as S^{2-} (in W−S−W structures) and as terminal and bridging S_2^{2-} ligands. Since the $\{WOS_2\}$ phase was formed by a simple thermal decomposition without applying special

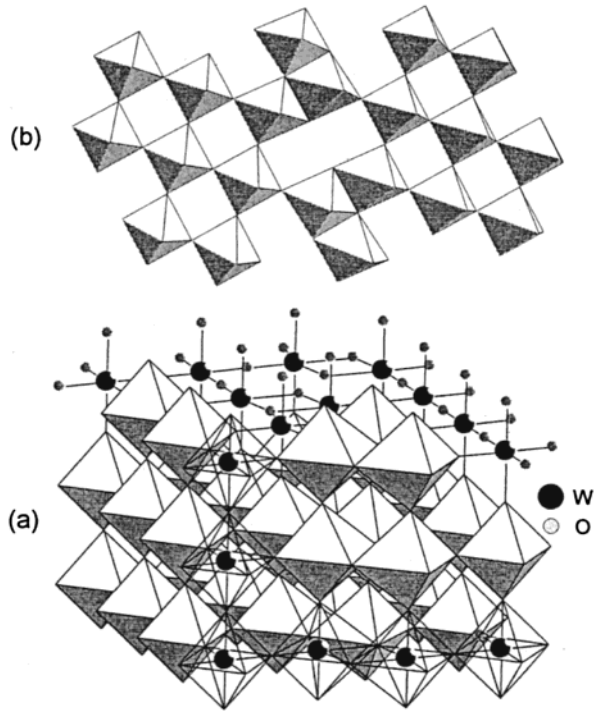

Figure 10. Structure of crystalline $W_{20}O_{58}$ (a) and projection of the unit cell showing the edge sharing of octahedra (b).

reaction conditions, we infer that the presence of oxygen and sulfur in the states and coordination modes mentioned above is a common structural property of tungsten oxysulfides. It is, therefore, likely that the tungsten oxysulfide intermediates of the sulfidation reaction with high S:W ratios also contain such structures. This assumption is in perfect agreement with our description of the sulfidation reaction thus far: The *shear oxysulfide* phase contains oxygen in terminal and bridging positions, and sulfur is present in the form of W═S (reaction 5) and W−S−W structures (reaction 9) and as terminal (reaction 7) disulfide ligands. The final step in the sulfidation of *m*-WO_3 is the transformation of the oxysulfide intermediate into WS_2. Some authors proposed {WS_3}-like intermediates in the sulfidation of tungsten-based hydrotreating catalysts.[36,37] This would mean that WO_3 is first sulfided up to high S:W ratios, followed by an adjustment of the stoichiometry to that of WS_2. However, in the case of the sulfidation of *m*-WO_3, the formation of an {WS_3}-like intermediate is very unlikely. A detailed discussion of this point can be found in ref 16. Therefore, the final step consists of the removal of oxygen from the oxysulfide and the final adjustment of the W:S ratio. This can proceed by means of the following reaction types. The first is an oxygen−sulfur exchange according to reaction 3 (W═O → W═S) with subsequent redox processes (reactions 7 and 8). In contrast to the W═O entities of *m*-WO_3, those of the oxysulfide are sufficiently reactive and undergo reactions with H_2S without additional activation of the W−O bond. Another possibility consists of the reaction of a W═O structure of the oxysulfide with H_2.

$$W^n{=}O_t + H_2 \rightarrow W^{(n-2)} + H_2O \qquad (11)$$

Such a reaction is not possible at an early stage of the sulfidation reaction due to the strong W−O bonds of *m*-WO_3. At this stage, however, the W−O bonds are weaker because of the lower formal oxidation state of the tungsten centers in the oxysulfide phase,[16] which is 5+ and 4+, and not 6+ as in *m*-WO_3. This, together with the higher temperature, makes the W═O fragments of the oxysulfide susceptible to a reaction with H_2 (reaction 11). The stepwise reduction of the tungsten centers from W^{VI} (in *m*-WO_3) to W^{IV} (in WS_2) via the above-mentioned W^V and $W^{V/IV}$ intermediate phases successively disfavors oxide structure types; from a certain degree of reduction of tungsten and a certain W−S stoichiometry, the WS_2 structure is thermodynamically favored. Terminal disulfide ligands, which are present in the tungsten oxysulfides but not in the WS_2 bulk structure, are removed by reductive elimination[38,39]

$$W^n{-}S_2 \rightarrow W^{(n-2)} + S_2(g) \qquad (12)$$

and by reactions with H_2[8]

$$W^n{-}S_2 + 2H_2 \rightarrow W^{(n-2)} + 2H_2S(g) \qquad (13)$$

The presence of microcrystalline WS_2 is indicated by the quick EXAFS data. After 30 min at 400 °C the EXAFS data show a W−S contribution at *2.0* Å, which is also found in the (not phase-corrected) Fourier transform of the k^3-weighted EXAFS function of macro crystalline 2H−WS_2 (not shown).

TABLE 2: Cell Parameters of Orthorhombic $WO_3{\bullet}H_2O$, $H_{0.10}WO_3{\bullet}H_2O$, and $H_{0.12}WO_3{\bullet}H_2O$

compound	*a* [Å]	*b* [Å]	*c* [Å]	ref
$WO_3{\bullet}H_2O$	5.249	10.711	5.133	12
$H_{0.10}WO_3{\bullet}H_2O$	5.256	10.659	5.222	40
$H_{0.12}WO_3{\bullet}H_2O$	5.251(5)	10.62(2)	5.233(6)	41

Sulfidation of $WO_3{\bullet}H_2O$. We will describe the sulfidation reaction of $WO_3{\bullet}H_2O$ and compare it with that of *m*-WO_3. The XRD pattern, obtained after sulfidation at 100 °C, is only slightly different from that of the starting material (Figure 3). Nevertheless, significant changes must have taken place, as indicated by the change in color from yellow to blue. The blue color suggests $W^{VI} \leftarrow W^V$ intervalence charge-transfer processes, in line with XPS measurements,[16] which showed that W^{VI} was partially reduced to W^V. This reduction does not go along with a significant incorporation of sulfur into the oxide lattice. Since these findings are similar to those of the sulfidation of *m*-WO_3, it is reasonable to anticipate that the first intermediate in the sulfidation of $WO_3{\bullet}H_2O$ is a tungsten bronze. Unfortunately, there are no data available on the interaction of H_2S with $WO_3{\bullet}H_2O$. However, two water-containing tungsten bronzes are known, i.e., $H_{0.10}WO_3{\bullet}H_2O$[40] and $H_{0.12}WO_3{\bullet}H_2O$.[41] Both bronzes are orthorhombic, as is $WO_3{\bullet}H_2O$ (Figure 7), with slight differences in their lattice parameters (Table 2). With respect to the positions of the heavy atoms, the structure of the bronzes is very similar to that of $WO_3{\bullet}H_2O$; thus the XRD patterns also differ only slightly. We therefore propose that the first intermediate in the sulfidation of $WO_3{\bullet}H_2O$ is a water-containing tungsten bronze of the type $H_xWO_3{\bullet}H_2O$. The value of *x* should be in the same order as for the above-mentioned examples. For this reason the formal composition of the first sulfidation bulk intermediate is $H_xWO_3{\bullet}H_2O$ ($x \approx 0.1$).

It is more difficult to unravel the next step. The quick EXAFS data (Figure 6) show that significant structural changes take place above 200 °C, which are also reflected in the powder diffraction data in Figure 2. XPS shows that sulfur is incorporated slowly into the surface of the oxide,[16] which is expected to proceed according to reactions 4 to 6. Since this alone does not explain the changes observed with quick EXAFS and XRD, we conclude that, parallel to the sulfidation of the surface, the bulk structure of the underlying oxide changes as well. Pure $H_xWO_3{\bullet}H_2O$, i.e., $H_xWO_3{\bullet}H_2O$ where no oxygen is replaced

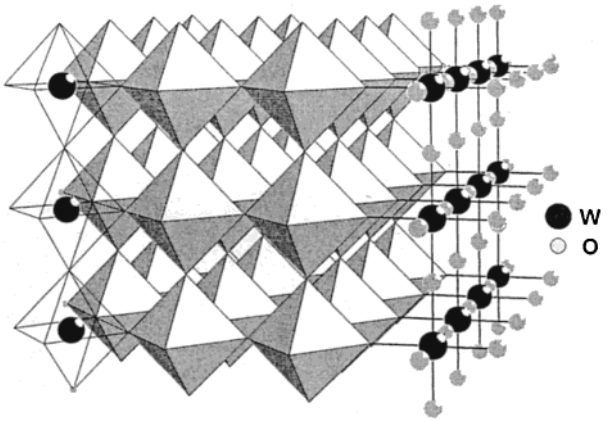

Figure 11. Structure of crystalline *c*-WO_3.

by sulfur, would most likely condensate to an oxide with a three-dimensional structure in agreement with the work of Yamaguchi et al.[42]

Yamaguchi et al. showed that $WO_3 \bullet H_2O$, as prepared by hydrolysis of $W(OEt)_6$ (Et = C_2H_5) transforms into cubic WO_3 upon heating in air.[42] This phase conversion takes place between 200 and 310 °C with simultaneous release of structural water and the condensation of [WO_6] octahedra of adjacent layers to form the three-dimensional structure of *c*-WO_3, which crystallizes in the ReO_3 structure and consists of nondistorted, corner-sharing [WO_6] octahedra, as is shown in Figure 11. Such a condensation process cannot take place if surface oxygen of the layered oxide is partially replaced by the larger sulfur, because, in that case, neighboring layers cannot be close enough. Indeed, XRD does not show the characteristic pattern of *c*-WO_3, which leads to the conclusion that $WO_3 \bullet H_2O$ transforms into *c*-WO_3 at 200 °C in air but not in an H_2S/H_2 gas mixture. Similar arguments are true for the $H_xWO_3 \bullet H_2O$ intermediate, the structure of which is similar to that of $WO_3 \bullet H_2O$ (vide supra). A transformation of this phase into a three-dimensional oxide structure type requires condensation of [WO_6] octahedra of neighboring layers and the loss of the structural water. Whereas the quick EXAFS data clearly show the release of structural water at around 200 °C, complete condensation does not occur. This means that some parts of the resulting phase are still layered, and its bulk structure is, therefore, probably that of a dehydrated tungsten bronze. The amount of hydrogen is typically higher in the case of bronzes without structural water (vide supra). We propose a bulk composition of H_yWO_3 ($y > x$) for the intermediate of the sulfidation of $WO_3 \bullet H_2O$ at 200 °C.

Although the reflections in the powder diffraction patterns obtained after sulfidation at 300 and 400 °C are broader than those in the patterns obtained at low sulfidation temperatures, the XRD pattern is in very good agreement with that of the shear oxide $W_{25}O_{73}$ (Figure 12). We therefore conclude that the first intermediate ($H_xWO_3 \bullet H_2O$) converts into a bronze of the type H_yWO_3, which subsequently transforms into $W_{25}O_{73}$. In this temperature range, the replacement of oxygen by sulfur (reactions 4−9) proceeds at a higher rate, so that the third intermediate phase is a *shear oxysulfide* of the formal composition $\{W_{25}O_{73-z}S_z\}$.

Above a certain S:W ratio, an oxysulfide phase forms which slowly transforms into WS_2 according to reactions 11−13. The presence of WS_2 is indicated by the contribution at *2.1* Å, which is due to the W−S distance as found in the (not phase-corrected) Fourier transform of the k^3-weighted EXAFS function of macro crystalline 2H−WS_2 (not shown).

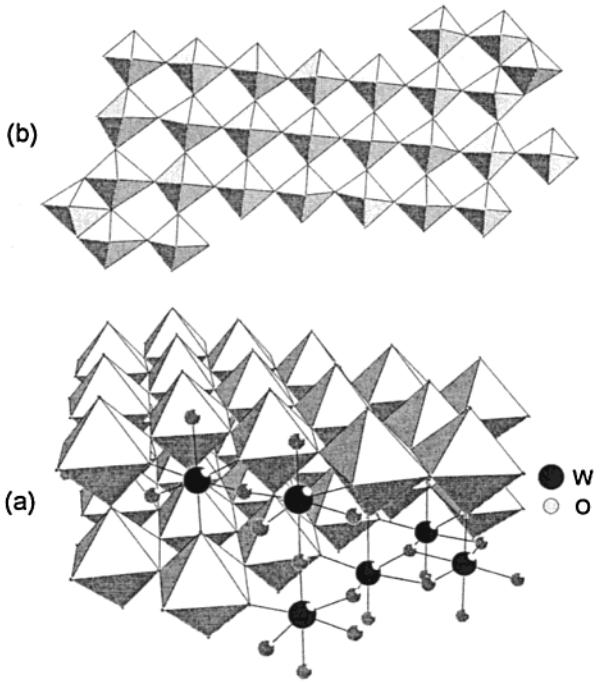

Figure 12. Structure of crystalline $W_{25}O_{73}$ (a) and a projection showing the edge sharing of octahedra (b).

Finally, there is an important difference between the sulfidation reactions of *m*-WO_3 and $WO_3 \bullet H_2O$. Whereas the general sequence is similar in both cases, i.e., oxide → bronze → *shear oxysulfide* → oxysulfide → sulfide, the degree of sulfidation is different. The intensity of the W−S contribution in the quick EXAFS spectra is much higher in the case of $WO_3 \bullet H_2O$, which suggests a higher degree of sulfidation and may imply a higher sulfidation rate. An important property that determines the rate of surface reactions is the surface area accessible to the reagents. Dickens et al.[43] determined the BET surface areas of *m*-WO_3 and $WO_3 \bullet H_2O$ (prepared by the method of Freedman[5]) to be 4.7 and 22.1 m^2/g, respectively, which corresponds to average particle sizes of 1800 and 500 Å, respectively. This difference in the average particle size is reflected in the powder diffraction data of *m*-WO_3 and $WO_3 \bullet H_2O$ (Figures 1a and 2a). The reflections in the XRD pattern of $WO_3 \bullet H_2O$ are broader than those of *m*-WO_3. Taking these data into account, the intrinsic rates of sulfidation are of a comparable order in both cases.

Conclusions

The results of the above discussion can be summarized as follows.

***m*-WO_3.**

1. The initial reaction at sulfidation temperatures below 100 °C is a reduction by H_2S to form the hydrogen tungsten bronze $H_{0.23}WO_3$.

2. Below 300 °C, the structure of the tungsten bronze is still intact but oxygen−sulfur exchange reactions (reactions 4−6) and W−S redox processes (reactions 7−9) take place.

3. Above 300 °C, reactions 4 to 9 take place in a more pronounced way on the surface of the particles, and the bulk structure changes from $H_{0.23}WO_3$ to that of the shear oxide $W_{20}O_{58}$, leading to the *shear oxysulfide* $\{W_{20}O_{58-x}S_x\}$.

4. Further incorporation of sulfur leads to oxysulfide intermediates with higher S:W ratios, which no longer have a *shear oxysulfide* structure and contain oxygen in terminal and bridging coordination types and sulfur as S^{2-} and S_2^{2-}. While S^{2-} is

mainly present in W−S−W structures, S_2^{2-} ligands predominantly occur in the terminal coordination mode.

5. The final step consists of the removal of oxygen from the oxysulfide and the final adjustment of the W:S ratio to form WS_2 by reactions 11 to 13.

$WO_3 \bullet H_2O$.

1. The first intermediate in the sulfidation reaction of $WO_3 \bullet H_2O$ is a tungsten bronze with the form $H_xWO_3 \bullet H_2O$ ($x \approx 0.1$), which forms at around 100 °C.

2. Below 300 °C, oxygen−sulfur exchange reactions (reactions 4−6) and W−S redox processes (reactions 7−9) take place on the surface, while the bronze dehydrates and a new bulk structure with the formal composition H_yWO_3 ($0.1 \ll y < 0.60$) forms.

3. At 300 °C, the bulk structure changes to that of the shear oxide $W_{25}O_{73}$ and, combined with reactions 4 to 9, the *shear oxysulfide* $\{W_{25}O_{73-z}S_z\}$ forms.

4. The *shear oxysulfide* $\{W_{25}O_{73-z}S_z\}$ slowly transforms into WS_2.

5. The rates of sulfidation are similar for both *m*-WO_3 and $WO_3 \bullet H_2O$.

In general, the sulfidation reaction starts at the surface of the particles while the bulk is still oxidic. Because of the high W−O bond energy, rather high temperatures are required to break the whole structure and to form a fully sulfided particle. This is the major reason full sulfidation of tungsten oxides can normally not be achieved below 400 °C.

References and Notes

(1) European Union, E. U. Directive 98/70/EC, 1998.

(2) Topsøe, H.; Clausen, B. S.; Massoth, F. E. In *Hydrotreating Catalyis, Science and Technology*; Eds. Anderson, J. R., Boudart, M., Springer-Verlag: New York, 1996; Vol. 11.

(3) Prins, R.; de Beer, V. H. J.; Somorjai, G. A. *Catal. Rev.—Sci. Eng.* **1989**, *31*, 1.

(4) McDonald, J. W.; Friesen, G. D.; Rosenhein, L. D.; Newton, W. E. *Inorg. Chim. Acta* **1983**, *72*, 205.

(5) Freedman, M. L. *J. Am. Chem. Soc.* **1959**, *81*, 3834.

(6) Cattaneo, R.; Weber, Th.; Shido, T.; Prins, R. *J. Catal.* **2000**, *191*, 225.

(7) Vaarkamp, M.; Dring, I.; Oldman, R.; Stern, E. A.; Koningsberger, D. C. *Phys. Rev.* **1994**, *B 50*, 7872.

(8) Diemann, E.; Weber, Th.; Müller, A. *J. Catal.* **1994**, *148*, 288.

(9) Weber, Th.; Muijsers, J. C.; van Wolput, J. H. M. C.; Verhagen, C. P. J.; Niemantverdriet, J. W. *J. Phys. Chem.* **1996**, *100*, 14144.

(10) Loopstra, B. O.; Boldrini, P. *Acta Cryst.* **1966**, *21*, 158.

(11) Magnéli, A. *Ark. Kemi.* **1950**, *1*, 513.

(12) Szymanski, J. T. *Can. Mineral.* **1984**, *22*, 681.

(13) Prasad, T. P.; Diemann, E.; Müller, A. *J. Inorg. Nucl. Chem.* **1973**, *35*, 1895.

(14) Leroy, M. J. F.; Kaufmann, G. *Bull. Soc. Chim. Fr.* **1968**, *9*, 3586.

(15) Nakamoto, K. *Infrared and Raman Spectra of Inorganic and Coordination Compounds*, 3rd ed.; Wiley: New York, 1978; p 135.

(16) Van der Vlies, A. J.; Kishan, G.; Niemantsverdriet, J. W.; Prins, R.; Weber, Th. *J. Phys. Chem. B* **2002**, *106*, 3449.

(17) Dickens, P. G.; Hurditch, R. J. *Nature* **1967**, *215*, 1266.

(18) Dickens, P. G.; Hurditch, R. J. In *Chem. Extended Defects Non-Metal. Solids Proc. Inst. Adv. Study*; Scottsdale: AZ, **1970**, *1969*, 555.

(19) Boudart, M.; Vannice, M. A.; Benson, J. E. *Z. Phys. Chem.* **1969**, *64*, 171.

(20) Benson, J. E.; Kohn, H. W.; Boudart, M. *J. Catal.* **1966**, *5*, 307.

(21) Hobbs, B. S.; Tseung, A. C. C. *J. Electrochem. Soc.* **1973**, *120*, 766.

(22) Ebert, F.; Flasch, H. *Z. Anorg. Allg. Chem.* **1936**, *226*, 65.

(23) Glemser, O.; Naumann, C. *Z. Anorg. Allg. Chem.* **1951**, *265*, 288

(24) Schwarzmann, E.; Birkenberg, R. *Z. Naturforsch.* **1971**, *26b*, 1069.

(25) Glemser, O.; Hauschild, U.; Lutz, G. *Z. Anorg. Allg. Chem.* **1952**, *269*, 93.

(26) Chevrier, J.; Siclet, G. *Bull. Soc. Chim. Fr.* **1976**, 1037.

(27) Siclet, G.; Chevrier, J.; Lenoir, J.; Eyraud, C. *Compt. Rend.* **1973**, *C 277*, 227.

(28) Vondrack, J.; Balej, J. *Collection Czech. Chem. Commun.* **1975**, *40*, 272.

(29) Dickens, P. G.; Moore, J. H.; Neild, D. J. *J. Solid State Chem.* **1973**, *7*, 241.

(30) Ampe, B.; Leroy, J. M.; Thomas, D.; Tridot, G. *Rev. Chim. Miner.* **1968**, *5*, 801.

(31) Harmer, M. A.; Sykes, A. G. *Inorg. Chem.* **1980**, *19*, 2881.

(32) Dickens, P. G.; Murphy, D. J.; Halstead, T. K. *J. Solid State Chem.* **1973**, *6*, 370.

(33) Müller, A.; Diemann, E. In *Comprehensive Coordination Chemistry*; Wilkinson, G., Gillard, R. D., McCleverty, J. A., Eds.; Pergamon: Oxford, 1987; Vol. II, Chapter 16.1.

(34) Magnéli, A. *Pure Appl. Chem.* **1978**, *50*, 1261.

(35) Massoth, F. E.; Bidlack, D. L. *J. Catal.* **1970**, *16*, 303.

(36) Payen, E.; Kasztelan, S.; Grimblot, J.; Bonnelle, J. P. *Catal. Today* **1988**, *4*, 57.

(37) Reinhoudt, H. R.; van der Meer, Y.; van der Kraan, A. M.; van Langeveld, A. D.; Moulijn, J. A. *Fuel Process. Technol.* **1999**, *61*, 43.

(38) Weber, Th.; Muijsers, J. C.; Niemantsverdiet, J. W. *J. Phys. Chem.* **1995**, *99*, 9194.

(39) Müller, A.; Weber, Th. *Appl. Catal.* **1991**, *77*, 243.

(40) Dickens, P. G.; Kay, S. A.; Crouch-Baker, S.; Claridge, D. A. *Solid State Ionics* **1987**, *23*, 9.

(41) Guéry, C.; Choquet, C.; Dujeancourt, F.; Tarascon, J. M.; Lassègues J. C. *J. Solid State Electrochem.* **1997**, *1*, 199.

(42) Yamaguchi, O.; Tomihisa, D.; Kawabata, H.; Shimizu, K. *J. Am. Ceram. Soc.* **1987**, *70*, C 94.

(43) Dickens, P. G.; Hibble, S. J.; Jarman, R. H. *J. Electron. Mater.* **1981**, *10*, 999.